Dyes and Pigments 199 (2022) 110044

Contents lists available at ScienceDirect

Dyes and Pigments

journal homepage: www.elsevier.com/locate/dyepig

Influence of substituents of Perylenebisimides on the surface energy and wettability: A systematic structure–property relationship analysis

M. Eugenia Pérez-Ojeda [a,*], Nathalie Zink-Lorre [b], Sara Pla [b], Andreas Zink [a], Ángela Sastre-Santos [b], Fernando Fernández-Lázaro [b,**], Andreas Hirsch [a,***]

[a] Department of Chemistry and Pharmacy, Friedrich-Alexander University of Erlangen-Nürnberg, Institute of Organic Chemistry, Nikolaus-Fiebiger-Str. 10, 91058 Erlangen, Germany

[b] Área de Química Orgánica, Instituto de Bioingeniería, Universidad Miguel Hernández, Avda. de la Universidad s/n, 03203, Elche, Spain

ARTICLE INFO

Keywords:
Perylene bisimide
Contact angle
Wettability
Surface energy
Substituents descriptors
QSPR quantitative structure-property relationship

ABSTRACT

This paper seeks to elucidate the influence on the surface wettability of a variety of substituents located in different positions of the perylene bisimide (PBI) core (ortho versus imide) with distinct electron-donor or -withdrawing character and diverse steric demand, using for this more than 20 planar PBIs. The correlation between the polarity of the individual functional group on the PBI and the surface wettability has been addressed by means of substituent descriptors in terms of Hansch-Fujita π parameter, Hammett σ_{meta} and σ_{para} constants, and steric parameters (Taft-Dubois Es' and Charton υ). With these parameters, a quantitative structure–property relationship (QSPR) analysis has been performed using multivariable linear regression (MLR) fittings. The relationship of Surface Energy, determined by the static contact angle method with three different solvents, to structural properties of PBIs is described. As well, the polar and dispersive contributions have been determined. For planar PBIs, a predominant influence of the substituents in the imide position on the surface wettability has been found despite of the electronic nature and steric hindrance of the substituents simultaneously located in ortho positions. This effect is more pronounced with the longer alkyl substituents at the imide position. This study paves the way for a rational chromophore design considering the on surface behavior, which will ultimately condition the contact and thus their performance in optoelectronic devices.

1. Introduction

Perylene bisimides (PBIs) have been widely investigated for optic and optoelectronic applications during the last decades thanks to their strong absorption of visible light, high fluorescence efficiency, n-type semiconducting character, and (photo-)stability, together with their relative easy synthetic methodology and numerous functionalization strategies [1] as well as the possibility to form tailored supramolecular structures [2]. Despite the widespread use of PBIs in high technological applications such as dye sensitized solar cells [3,4], organic light-emitting diodes (OLEDS) [5,6], lasers [7], singlet fission [8,9], photocatalysis [10–12], water splitting [13], supramolecular exfoliation [14], 2D materials surface passivation [15,16], gene vectors [17], bio-imaging [18], sensing and pollutant degradation [19], among others [20], a systematic study on their wettability which determines the interfacial interactions and therefore ultimately condition the devices' efficiency is still lacking. Surface wettability plays an important role as well in many functional applications such as superhydrophobic self-cleaning materials, antifouling surfaces, corrosion protection and fluid control [21]. Thus, understanding the influence of PBIs structure, nature of their side chains and substitution positions on the surface wettability is of great interest.

Few studies address the wettability of some individual perylene mono- [22] and bisimide derivatives [23,24] or PBI-coated surfaces [25–28] highlighting the influence of the substituents in the contact angle and surface interaction, which plays a crucial role in the final device performance as shown in these examples. To the best of our knowledge there is only one short systematic study including six PBI

; PBI, Perylene bisimide; QSPR, Quantitative structure-property relationship; MLR, Multivariable linear regression.

* Corresponding author.
** Corresponding author.
*** Corresponding author.
E-mail addresses: eugenia.perez-ojeda@fau.de (M.E. Pérez-Ojeda), fdofdez@umh.es (F. Fernández-Lázaro), andreas.hirsch@fau.de (A. Hirsch).

https://doi.org/10.1016/j.dyepig.2021.110044
Received 9 September 2021; Received in revised form 16 December 2021; Accepted 17 December 2021
Available online 21 December 2021

derivatives with different imide substituents which focus on the structure-wettability relationship [29]. Nevertheless, far from helping in the understanding, it confuses by its counter-intuitive conclusions. Strikingly, in this work highly hydrophilic contact angles ranging from 13.8 to 36.0° are described for core-unsubstituted PBIs bearing hydrophobic aliphatic chains such as nonan-5-yl, undecan-6-yl and n-butyl at the imide positions. These values are far from the ones that we have measured for very similar structures. Aware of the lack of studies in this regard, and moved by the ever increasing applicability of PBIs, herein we carried out a deep systematic study including 22 PBI derivatives bearing various substituents with different electron-donor or -withdrawing character and diverse steric demand at different positions of the PBI (ortho versus imide). A QSPR analysis on the surface wettability and surface energy will pave the way for guiding the molecular design of PBIs in order to efficiently modifying the interfacial condition, thus optimizing final device performance.

2. Results and discussion

2.1. Substituents influence in surface wettability

A set of 22 PBI derivatives has been synthesized and classified for their analysis in four different series attending to their structural characteristics (Fig. 1). Thereby, series 1 compares different substituents at imide position of planar core-unsubstituted PBIs. Substituents bearing alkyl chains of different length and symmetry (compounds **1**, **2, 4** and **6**), perfluorinated chain (**5**) and an arylalkylcarboxylic acid (**7**) are examined. Series 2 includes the same unsubstituted core structure type but focuses on polarity, comparing an alkylamino chain with the N-oxide and ammonium salts with different counterions derived from it. Series 3 and 4 compare planar PBIs with different substituents in ortho positions and the same group at the imide: N-pentan-3-yl and *N*-tridecan-7-yl, respectively. The ortho substitution was preferred over the bay position to preserve the planarity of the PBI core and therefore have a more comparable geometry to that of the unsubstituted ones. Moreover, distorted tetrachloro bay substituted PBI **10** has been included for comparison to see the influence of the core twisting (dihedral angle of 36.7°) [30] with the same substituents. Some ortho-substituents are able to form H bonds (**11**, **18**, **19**), others are electron donating (**11**, **12**, **15**, **17**–**19**), electron withdrawing (**8**–**10**, **13**) or bear very bulky groups (**12**). Therefrom, along these four series, the steric effects, electronic contributions and lipophilicity, which have a significant impact on the wettability and surface tension, are analyzed.

Two different deposition methods (drop casting and spin coating) have been compared with series 1 and 4 to consider possible contributions of some sort of surface nano-structure due to self assembly or aggregation during the drying process that might affect the resulting angle. The differences are more significant in series 1 probably due to the unsubstituted perylene core that allows an easier interchromophoric interaction via π-π stacking and self assembly on the surface. It is well known that surface roughness through micro- and nano-structuration lowers the surface energy and increases the hydrophobicity [31]. In fact, this strategy is generally used for making anti-wetting surfaces. The differences observed in series 4 are minor. As expected, for both series, the experimental angles are slightly higher for the drop casting method than for the spin coating deposition (except for compounds **4** and **7** where the higher steric demand of the substituent in the imide position might be preventing their self-organization). Presumably, the slower evaporation rate in the drop casting method allows for a better molecular self-arrangement. Regarding this, the spin casting method should be preferred to eliminate the contribution of the surface structuration. However, the drop-casting method was chosen as better coverage was reached and the statistics of different measures was more consistent (for more information see SI, Tables S3 and S4). Nevertheless, very volatile solvents such as dichloromethane and methanol were employed to minimize the drying time and thus the self-assembly process.

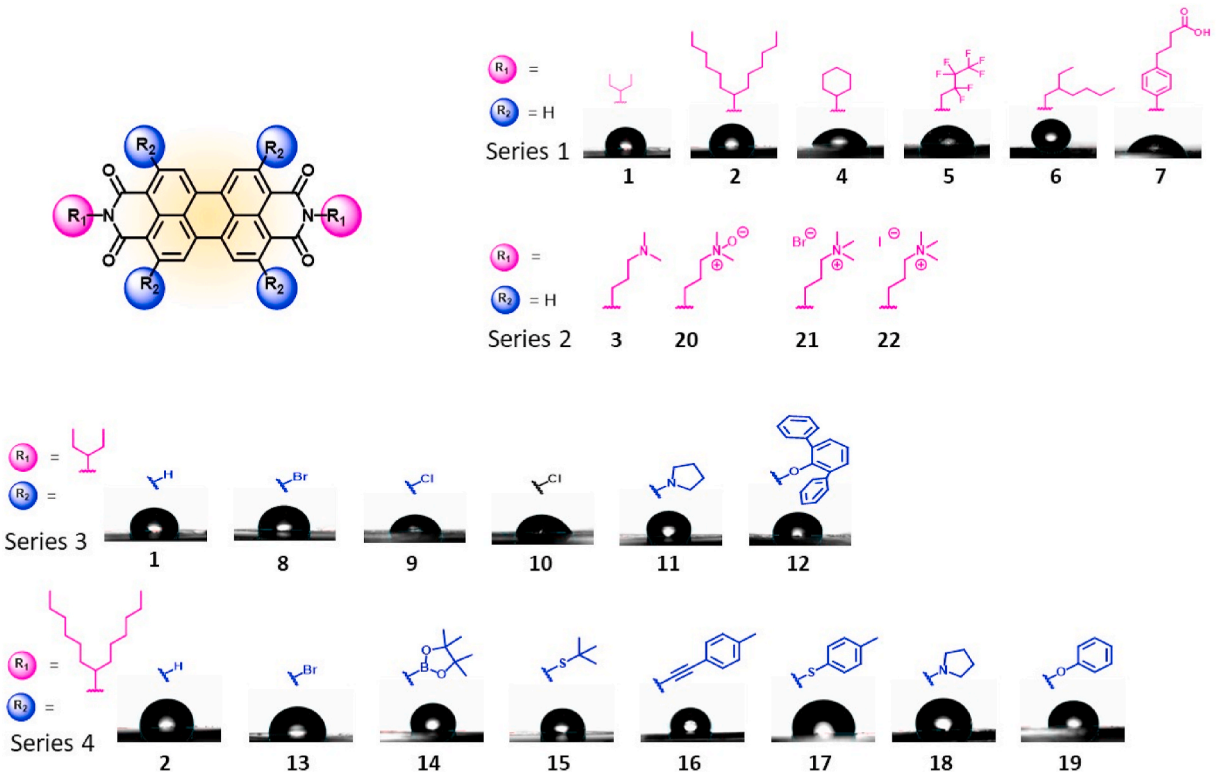

Fig. 1. Chemical structure of 22 PBIs analyzed in this study. The substituents at imide position are marked in pink and the ones at ortho in blue. The bay substituted one (**10**, with $R_2 = H$) has been highlighted in black for clarification purposes. Images of the static contact angle in water are also included. (For interpretation of the references to color in this figure legend, the reader is referred to the Web version of this article.)

The static contact angles were evaluated in three different solvents to allow the further calculation of the surface energy. Water (as polar solvent), ethylenglycol (EG) and diiodomethane (methylene iodide, MI) (as non polar) were chosen in all cases except for series 2, where formamide (partially polar) was used due to the high solubility in water of the polar perylenes. The polar and disperse components of the surface energies were obtained by the Owens–Wendt–Rabel–Kaelble (OWRK) model [32] (for experimental details see SI, tables S2 and S5-S8). The results are summarized in Tables 1 and 2. For series 1, the contact angle values in water range from 62.49° to 129.86°. The most hydrophilic one is compound **7** bearing arylalkylcarboxylic acid chains able to form hydrogen bonds, with a value of 62.49°, in very good agreement with other carboxy PBIs described in the literature which exhibit values from 58° to 67° [25]. Hydrophobic derivative **6** bearing an aliphatic swallow tail shows the highest angle of 129.86° which is close to the values described for structurally similar asymmetric PBI on silica [28] and PMI with long alkyl chains at the imide position (118.6° and 112.3°, respectively) [22]. The water contact angle for series 2 could not be evaluated due to experimental limitations. These derivatives are soluble in water, which prevents the measure since the drop dissolves the PBI film immediately after deposition. Nevertheless, the high hydrophilicity of these derivatives is as well in agreement with the contact angle described for a similar amphiphilic zwitterionic PBI with 28° angle [24]. Despite their structural diversity, series 3 and 4 present more uniform values ranging from 78.41° to 111.50°. This fact is related to the substitution position (ortho-), which influences the wettability to a lesser extent than the substitution at the imide position, as it will be concluded from this study.

To further rationalize the correlation between the polarity of the individual functional group on the PBI and the surface wettability in a quantitative manner, the results with water have been analyzed by means of substituent parameters. As descriptors, Hansch-Fujita π parameter (related to the octanol/water partition coefficient and therefore to the substituent contribution to the lipophylicity), Hammett σ_{meta} and σ_{para} constants (indicative of the electronic effect of substituents on an aromatic ring at meta or para position, respectively), and steric effects (Taft-Dubois and Charton) have been employed.

In order to discriminate the more influencing substitution positons, initially, monovariable analysis to observe the tendencies and correlation of each parameter to the wettability and surface energy have been addressed. Secondly, multivariable linear fittings were performed for a proper quantification. Contact angles were plotted as a function of calculated σ_{meta}, σ_{para} and π values [33] or as function of Es' or υ values extracted from the indicated references. [34–37]. Each series was analyzed with different descriptors depending on their structure. Series 1 and 2 were not analyzed in terms of electronic parameters (Hammet σ_{meta}, σ_{para}) since they refer to substituents located in the aromatic core which is not applicable at the imide position. Lipophylicity trough Hansch-Fujita descriptor π allowed us to compare most of the compounds. Unfortunately, series 2 could not be analyzed in terms of wettability since no values for the water contact angle can be obtained due to their solubility, yet the surface energy as well as dispersive and polar components could be calculated and compared to all others in a global analysis.

2.1.1. Lipophylicity in series 1, 3 and 4: Hansch-Fujita π parameter

The representation of the contact angle against π (Fig. 2) clearly demonstrates that the greatest influence of lipophylicity occurs in series 1 (Fig. 2a). On the other extreme lies series 4, where the π values of the substituents show no effect on the observed contact angles (Fig. 2c). This can be attributed to the long alkyl chains on the imide positions which dominate the lipophilic character of the molecules. Series 3 (Fig. 2b), with alkyl chains shorter than in series 4, shows a light contribution of the ortho substituents to the total lipophylicity of the molecule. The lipophylicity of the substituents (expressed in terms of Hansch-Fujita parameter) has only a determinant contribution to the total compound hydrophobicity, and therefore to the contact angle, when the substituents are located at the imide position (series 1). This is probably because of the planar geometry of these PBIs where the imide substituents will be pointing outwards, exposed towards the surface and influencing much more the surface behavior. Orientation and self-assembly of rylene bisimides on surface have received great attention within the last years [2,38]. Depending on the interaction with the substrate, the orientation might be flat with "face on" organization driven by π-π interactions as in graphene, melamine, or black phosphorus coatings [39], self-assembled monolayers (SAMs) with the perylene cores perpendicular to the surface when using high packing densities [25] or on a tilted "edge-on" structure [40]. In all cases, the imide substituents will be pointing outwards interacting with the surface and therefore will play a crucial role in the wettability. It is well stablished that substitution at imide position has negligible effects on absorption and emission properties since the frontier orbitals HOMO and LUMO possess a node at the imide nitrogen, therefore, the substituents are electronically decoupled from the aromatic core. However, for the on surface behavior, our study demonstrates that the substituents placed at the imide position are the ones with the greatest influence on the wettability.

A trend is noticed between lipophilicity (π) and the contact angle for series 1, a greater contact angle is observed corresponding to a more hydrophobic character and higher π values of the imide substituent. A deeper analysis of the differences in series 3, where both the imide and ortho substituents take part, suggests the contribution of some other factors, as compounds **8**–**11** show quite different angles for a close π value (but different electron-donating/accepting character, vide infra),

Table 1
PBIs static contact angles from series 1 and 2 evaluated in three different solvents and the resultant surface energies and dispersive and polar components. Substituent descriptors have been calculated or obtained from the indicated references. a) By analogy with $CH(n\text{-}Bu)_2$ b) By analogy with CF_3. c) By analogy with CH(Et) (n-Bu). d) The counterion was not considered in π calculation.

	π [33]	Es' [34]	υ [35,36]	Static contact angle θ			SE Components [mN/m]		
Series 1				Water	EG	MI	Υ^{total}	Υ^{d}	Υ^{p}
1	2	−2	1.51	100.11	65.07	41.56	43.30	43.18	0.13
2	6.15	−2.08[a]	1.56[a]	97.56	70.50	49.62	35.52	35.48	0.04
4	2.161	−0.69	0.87	66.43	58.39	40.43	37.39	27.94	9.45
5	2.463	−0.78[b]	0.91[b]	74.63	65.09	58.21	29.97	20.81	9.16
6	3.448	−2.03[c]	1.55[c]	129.86	97.86	54.83	49.40	41.38	8.02
7	2.167	–	0.57 [37]	62.49	43.85	49.06	39.50	24.17	15.33
Series 2				**Formamide**	**EG**	**MI**			
3	0.557	–	–	51.13	38.68	40.43	42.81	35.27	7.54
20	−1.993	–	–	69.64	67.71	51.79	37.71	37.62	0.08
21	−3.421[d]	–	–	22.58	28.17	26.47	49.96	34.26	15.70
22	−3.421[d]	–	–	18.06	25.95	26.02	50.85	33.96	16.99

Table 2
PBIs static contact angles from series 3 and 4 evaluated in three different solvents and the resultant surface energies and dispersive and polar components. Substituent descriptors have been calculated using an specific software [33].

	σ_{meta}	σ_{para}	π	Static contact angle θ			SE Components [mN/m]		
Series 3				Water	EG	MI	ϒtotal	ϒd	ϒp
1	0	0	0	100.11	65.07	41.56	43.30	43.18	0.13
8	0.392	0.282	0.967	96.65	74.27	53.39	32.00	31.80	0.19
9	0.378	0.2	0.836	78.41	64.04	45.71	33.82	29.57	4.25
10	0.378	0.2	0.836	71.20	53.21	44.86	36.67	28.53	8.03
11	−0.214	−0.718	0.663	111.50	90.62	28.62	55.19	50.46	4.73
12	0.111	−0.23	5.406	98.40	71.39	45.47	38.37	38.36	0.01
Series 4									
2	0	0	0	97.56	70.50	49.62	35.52	35.48	0.04
13	0.392	0.282	0.967	94.93	71.79	50.60	33.49	33.23	0.26
14	0.008	0.097	1.235	109.75	84.43	60.20	31.81	31.42	0.40
15	0.023	0.017	1.941	100.37	76.77	59.80	29.03	28.90	0.13
16	0.198	0.122	2.15	98.47	76.56	57.89	29.51	29.31	0.21
17	0.174	0.028	2.738	100.51	73.54	43.54	40.37	40.22	0.15
18	−0.214	−0.718	0.663	105.76	80.21	38.39	46.05	44.64	1.41
19	0.138	−0.166	1.912	95.59	75.01	62.85	26.17	25.11	1.05

Table 3
MLR for the surface energies (black) and dispersive (blue) and polar (orange) components using the different substituents descriptors. The goodness of fitting in terms of r^2 is also included.

Series 1 (**1**, **2**, **4**, **5** and **6**)	$\Upsilon^{total} = 21.7973 - 2.6344\ \pi + 20.2077\ \upsilon$	$r^2 = 0.67$	Eq. 8
	$\Upsilon^{D} = 3.7413 - 2.3109\ \pi + 29.3079\ \upsilon$	$r^2 = 0.92$	Eq. 9
	$\Upsilon^{P} = 18.0521 - 0.3257\ \pi - 9.0900\ \upsilon$	$r^2 = 0.54$	Eq. 10
Series 3 (**1**, **8**, **9**, **11** and **12**)	$\Upsilon^{total} = 46.1761 - 34.6049\ \sigma_m - 0.6503\ \pi$	$r^2 = 0.96$	Eq. 11
	$\Upsilon^{D} = 43.4235 - 32.6207\ \sigma_m - 0.2527\ \pi$	$r^2 = 0.99$	Eq. 12
	$\Upsilon^{P} = 2.7553 - 1.9987\ \sigma_m - 0.3980\ \pi$	$r^2 = 0.18$	Eq. 13
Series 4 (**2**, **13-19**)	$\Upsilon^{total} = 35.1426 - 12.0518\ \sigma_p - 1.1429\ \pi$	$r^2 = 0.37$	Eq. 14
	$\Upsilon^{D} = 34.7913 - 10.6215\ \sigma_p - 1.1727\ \pi$	$r^2 = 0.32$	Eq. 15
	$\Upsilon^{P} = 0.3538 - 1.4231\ \sigma_p + 0.0292\ \pi$	$r^2 = 0.72$	Eq. 16

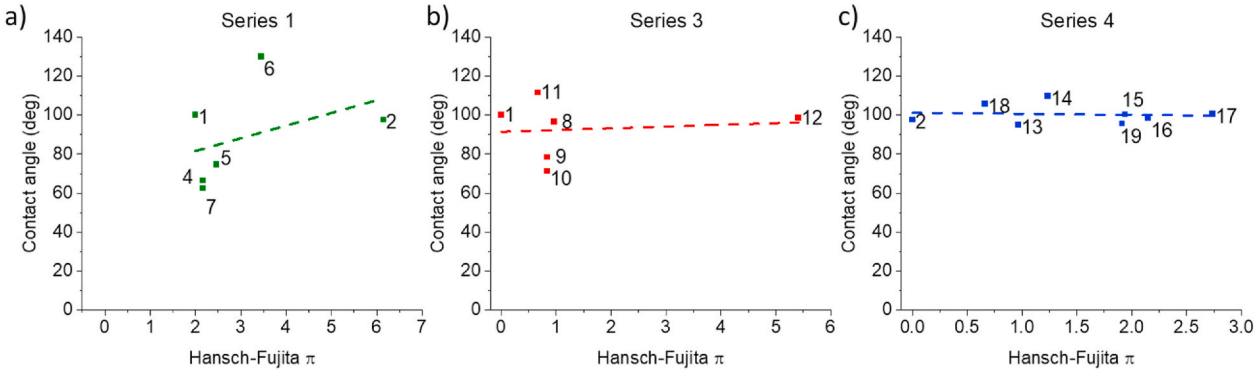

Fig. 2. Contact angles versus Hansch-Fujita lipophilic π parameter for series 1 (a), 3 (b) and 4 (c). The labels correspond to each compound number.

while compounds **1** and **12** display similar angles for a very different steric hindrance. A direct comparison between ortho- and bay substitution can be made with compounds **9** and **10**, where the bay substituted PBI is more affected displaying more hydrophilic contact angles probably due to the nonplanar structure caused by the bay substitution.

2.1.2. Series 1: steric parameters Taft-Dubois Es' and Charton υ

Es' stands for a revised definition by Dubois of Taft steric effects of the substituents on a certain reaction rate defined on the basis of more unified reactions and over a wider range of substituent. The values decrease with increasing steric bulkiness being 0 for methyl. On the other hand, Charton parameter is defined based on the substituent size by assuming the Van der Waals radius as atom contour. Plotting the contact angles versus the available Es' values from literature shows a clear trend where the bulkier groups exhibit also the higher angles and therefore are the more hydrophobic (Fig. 3a). This trend is also reflected in Charton's analysis (Fig. 3b). Unfortunately, the experimental values for these descriptors are very scarce and difficult to predict, thus the analysis could only be done with series 1. Nonetheless, since the substituents located at the imide position are the ones affecting more the overall hydrophobicity, this series is the most representative one to consider this effect.

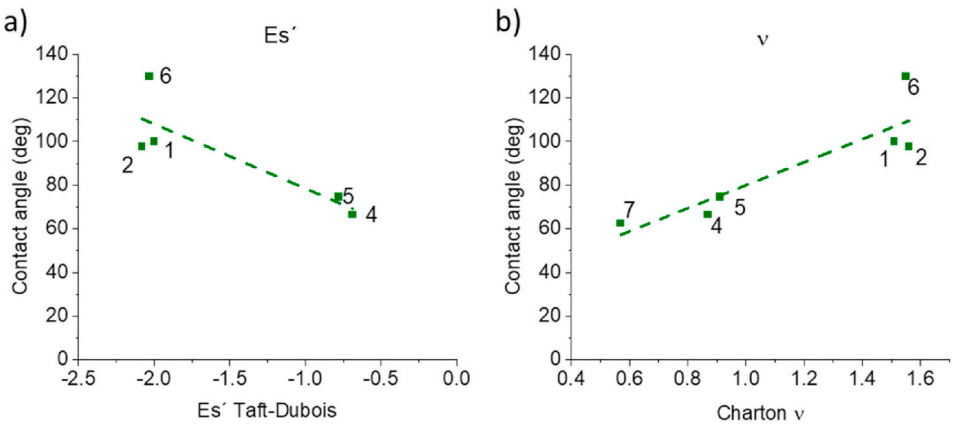

Fig. 3. Influence of steric parameters a) Taft- Dubois and b) Charton descriptors on surface wettability for series 1.

2.1.3. Series 1: Combined lipophilic and steric parameters

For a quantitative analysis, multivariable linear regressions (MLRs) for series 1 including π and Es' or υ alternatively, were calculated (equations (1) and (2)). Equation (1) was calculated considering compounds **1**, **2**, **4**, **5** and **6** and equation (2) with **1**, **2**, **4**, **5**, **6** and **7**. They demonstrate a good correlation of the observed contact angles with the lipophilic and steric parameters of the substituents at the imide positions (regression coefficients, r^2, 0.75 for Es' and 0.80 for υ). It is interesting to note that steric factors of the substituents seem to be more influential on the contact angle than their lipophilicity, as deduced from the coefficients in equations (1) and (2).

$$\bullet\ \theta = 52.2530 - 2.6283\,\pi - 32.9765\,Es' \quad r^2 = 0.75 \qquad \text{(Eq. 1)}$$

$$\bullet\ \theta = 28.6546 - 2.3005\,\pi + 57.5977\,\upsilon \quad r^2 = 0.80 \qquad \text{(Eq. 2)}$$

Using these equations and introducing the corresponding substituents descriptors (π, Es'or υ) allows the prediction of θ values for other planar PBIs with substituents at the imide position, which can be very useful in guiding the molecular design to fulfill the specific application requirements.

2.1.4. Series 3 and 4: electronic parameters Hammet σ_{meta} and σ_{para} constants

The electronic contribution of the substituents to a given process depends on their relative position with respect to the reaction center. As in present case we are dealing with a property of the whole molecule rather than with an effect in a localized point, we will try to correlate the contact angles with either σ_{meta} or σ_{para}, to elucidate which is the most appropriate parameter to be used. The σ constants are relative to hydrogen and they have been calculated using the same specific software for quantitative structure-activity relationship QSAR analysis that was previously mentioned for the estimation of π [33]. The experimental contact angle values show certain correlation to Hammett σ-constants of the respective substituents. Electron-withdrawing substituents have a positive σ value and PBIs bearing these substituents display generally smaller and therefore more hydrophilic contact angles (see Fig. 4 and Table 2).

The partial analysis considering series 3 and 4 shows again the same behavior that the analysis of Hansch-Fujita parameter where series 3 is more sensitive to the substituent variation than series 4. Thus confirming the strong influence of long alkyl substituents at the imide positions: the overall hydrophobicity in series 4 is dominated by the tridecan-7-yl substituent instead of the substituents located in ortho. The foregoing is equally applicable to both σ_{meta} and σ_{para} (Fig. 4 a and b).

2.1.5. Series 3 and 4: Combined lipophilic and electronic parameters

The quantitative analysis using these descriptors for series 3 and 4 demonstrated a worst correlation than in equations (1) and (2). For series 3, MLR analysis using compounds **1**, **8**, **9**, **11** and **12** afforded equations (3) and (4). The slightly higher regression coefficient value for eq. (3) may indicate that the electronic effects of substituents in ortho positions are better approximated using σ_m parameters. Moreover, the electronic effects play a more important role than the lipophilic ones. In any case, the effect of the substituents are much weaker than the effect of the substituent at the imide position represented by the parent compound **1** (intercept value).

$$\bullet\ \theta = 101.6825 - 38.1996\,\sigma_m + 0.2714\,\pi \quad r^2 = 0.68 \qquad \text{(Eq. 3)}$$

$$\bullet\ \theta = 95.8131 - 23.0753\,\sigma_p - 0.6032\,\pi \quad r^2 = 0.59 \qquad \text{(Eq. 4)}$$

On the other hand, carrying MLR analysis with compounds **2** and **13**–**19**, corresponding to series 4, led to equations (5) and (6). In this case, r^2 values are very low, indicating a poor correlation between contact angles and the used parameters. As in the previous series, the

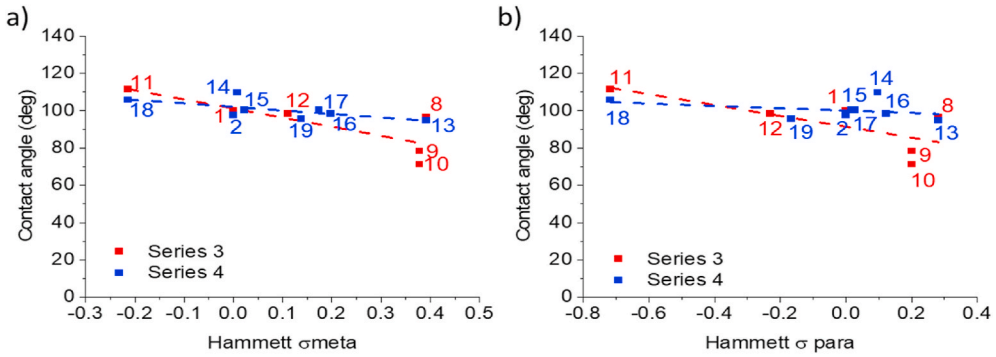

Fig. 4. Influence of electronic parameters, a) σ_{meta} and b) σ_{para}, descriptors on surface wettability for series 3 and 4.

electronic effects are more important than the lipophilic ones, and σ_m parameters yield a somehow better description than σ_p parameters. Comparing the coefficients in equations (3) and (5) (or in equations (4) and (6)), it is clear that the substituents'effect is much lower in series 4.

$$\bullet\ \theta = 100.7607 - 20.7200\ \sigma_m + 1.0126\ \pi \quad r^2 = 0.47 \qquad \text{(Eq. 5)}$$

$$\bullet\ \theta = 100.1206 - 6.1936\ \sigma_p - 0.0102\ \pi \quad r^2 = 0.13 \qquad \text{(Eq. 6)}$$

2.2. Substituents influence in surface energy

The wetting thermodynamics was experimentally investigated by analyzing dispersive and polar component surface energies using the Owens–Wendt–Rabel–Kaelble (OWRK) method represented by equation (7), where D and P are the dispersive and polar components, respectively, of the solid surface energy (ϒS) or the liquid surface tension (ϒL) and θ is the contact angle. Thus, the polar and dispersive contributions to the total surface energy could be calculated (Tables 1 and 2). Surface tension and its components for model liquids used in the calculations (water, formamide, ethylenglycol and diiodomethane) can be found in the SI (Table S2).

$$\gamma_L\Delta(1+cos\theta) = 2\Delta\left(\sqrt{\gamma_S^D\Delta\gamma_L^D} + \sqrt{\gamma_S^P\Delta\gamma_L^P}\right) \qquad \text{(Eq. 7)}$$

The cohesion between the molecules that causes the surface energy of a material can be explained by dispersive and polar contributions. Interactions caused by temporary fluctuations of the charge distribution in the atoms/molecules are called dispersive interactions (London dispersion force). Polar interactions comprise Coulomb interactions between permanent dipoles and between permanent and induced dipoles (e.g. hydrogen bonds). The surface energy is additively made up of such dispersive and polar parts. Because Van der Waals interactions occur between all atoms and molecules there is no substance with a surface energy/tension that solely consists of a polar part. Indeed, a predominant dispersive character of surface energy was measured for all PBIs (Fig. 5). Moreover, polar contributions were only significant in series 1 and 2 especially for PBIs bearing groups with the higher electrondonating, electronwithdrawing and polar character (PBIs with perfluorinated tail **5**, carboxylic acid **7**, tertiary amines **3**, **11**, chlorine **9**, **10** and quaternary ammonium salts **21** and **22**). These results are in agreement with our previous discussion on substituents descriptors where the most affected series were the ones with the substituent at the imide position (Series 1 and 2) followed by series 3 with a subtle influence of the ortho substituents. This influence is completely negligible in series 4 where the long swallow tail chain oriented towards the contact surface dominates the interaction and promotes an homogeneous behavior form very different PBIs. Thereby, there is practically no polar contribution of the substituents to the total surface energy in series 4 as in unsubstituted PBI **2**. Interestingly, the comparison of derivatives **11** and **18** having the same pyrrolidine substituents, which should have some polar contributions, leads us again to the conclusion that the long alkyl substituents located at the imide position in series 4 govern the surface interaction and veil the ortho contribution. Consequently, derivative **11** has a polar contribution of 4.73 mN/m meanwhile derivative **18** only have 1.41 mN/m of polar component.

However, some exceptions are not completely fitting the trend, probably because the energetic differences that are being described here are minuscule. Derivatives **4** and **6** are not following the correlation with the chemical composition since their substituents are alkanes and should have only dispersive contributions. Thus, the respective polar contributions of 9.45 mN/m and 8.02 mN/m are unexpected although their magnitude is low at the energetic scale. On the opposite side, derivative **20** has an unexpected low polar component, as it would have been expected for the amine oxide, which should be closer to the ammonium salts component distribution for **21** and **22**. The unraveling of this result is out of the scope of this article and will be pursued in next studies.

The surface energy values (Fig. 5 and Tables 1 and 2) indicate that most PBIs are low-surface energy materials (below 36 mN/m) and only few of them can be included in the medium surface energy range (from 36 to 300 mN/m). The value of 29.97 mN/m for the perflourinated PBI **5** is slightly higher than the Teflon surface energy (PTFE 24.01 mN/m) [41] but nevertheless in good agreement with other surface functionalized materials like indium-tin oxide electrodes, titanium dioxide or aluminiun oxide nanoparticles functionalized with perfluorinated tails (energies ranging from 6 to 35 mN/m depending on the grafting density) [42]. Chlorinated PBIs **9** and **10** with energy values of 33.82 and 36.67 mN/m, respectively, are in good agreement with the described values for PVC polymers (35–39 mN/m depending on the plasticizers) [43]. Furthermore, the comparison of derivatives **9** and **10** evidences again the fact the planar distortion affects the surface behavior since a higher polar contribution is observed in the non planar bay substituted compound **10**.

MLRs were also calculated for the surface energy and the corresponding components (Tables 3 and SI, Table S9). For series 1 the dispersive effects show a good correlation with the studied parameters (Eq. (9)), while the surface energy and, especially, the polar effects show a poorer fit (Eqs. (8) and (10)). In all three equations, the steric factors dominate over the lipophilic ones.

For series 3, the fit of the experimental values of surface energy and dispersive effects to σ_m and π is very impressive, while for the polar effects is rather poor. As observed previously (Eq. (3) vs Eq. (4) and Eq. (5) vs Eq. (6)), the electronic effects of substituents in ortho positions are better approximated using σ_m parameters (See Eqs.(11)-(13) using σ_m vs

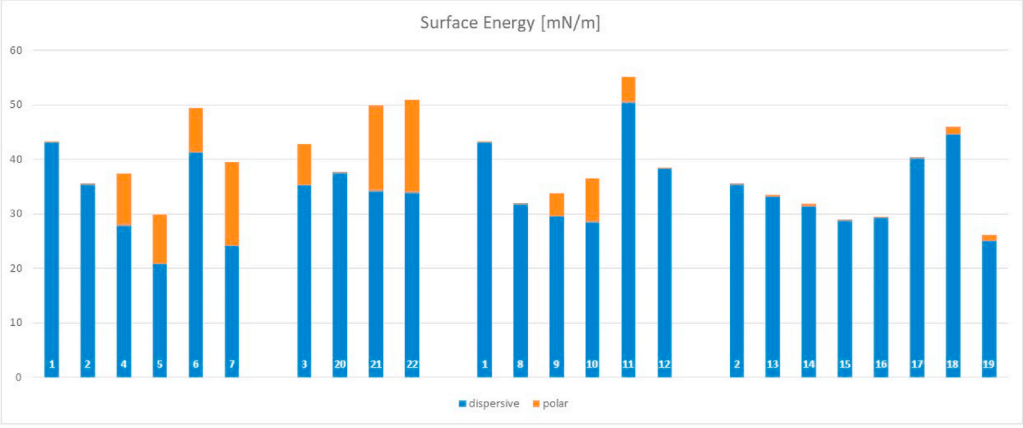

Fig. 5. Bar diagram corresponding to the surface energies of the 22 PBIs. The dispersive contribution is shown in blue and the polar one in orange. (For interpretation of the references to color in this figure legend, the reader is referred to the Web version of this article.)

Eqs (20)–(22) in SI using σ_p). Moreover, the electronic effects seem to have much more influence in ϒ than the lipophilic ones, and are in a similar order of magnitude as the effect of the substituent at the imide position represented by the parent compound **1** (intercept value).

Finally, series 4 shows bad fittings, with the exception, maybe, of the polar effects. In these equations σ_p seems to provide a better adjustment, but the regression coefficients (r^2) are so low that a conclusion on this item can be hardly extracted.

3. Materials and methods

Reagents and solvents were purchased from commercial sources and used without further purification. Column chromatography: SiO_2 (40–63 μm). TLC plates coated with SiO_2 60F254 were visualized by UV light. NMR spectra were recorded at 25 °C using a Bruker AC300 spectrometer. The solvents for spectroscopic studies were of spectroscopic grade and used as received. UV/vis spectra were measured with a Helios Gamma spectrophotometer. IR spectra were recorded with a Nicolet Impact 400D spectrophotometer. High-resolution mass spectra were obtained from a Bruker Reflex II matrix-assisted laser desorption/ionization time-of-flight (MALDI-TOF) spectrometer using dithranol as matrix or from a Bruker MicrOTOF using Electrospray ionization (ESI).

PBIs **1** [44], **2** [44], **3** [45], **4** [44], **5** [46], **6** [47], **7** [48], **10** [49], **13** [50], **14** [51], **15** [52], **17** [52], **19** [52], **20** [53], and **22** [45], were synthesized according to reported procedures.

Synthesis of N,N′-di(ethylpropyl)-2,5,8,11-tetrabromoperylene-3,4:9,10-bis(dicarboximide) (**PBI 8**).

A mixture of dioxane (100 mL), methanol (20 mL) and water (10 mL) was added, under inert conditions, to *N,N′*-di(ethylpropyl)-2,5,8,11-tetra(4′,4′,5′,5′-tetramethyl-1′,3′,2′-dioxaborolan-2′-yl)perylene-3,4:9,10-bis(dicarboximide) (500 mg, 0.48 mmol) and $CuBr_2$ (2.255 g, 0.01 mol). The reaction was refluxed 16 h at 120 °C, and after cooling, it was extracted with toluene. The organic layer was dried over anhydrous sodium sulfate, filtered and evaporated. Purification was carried out by silica gel column chromatography using dichloromethane as eluent.

Yield: 55% (225 mg); orange solid; ^{1}H NMR (300 MHz, $CDCl_3$) δ 8.73 (s, 4H), 5.06 (m, 2H), 2.17 (m, 4H), 1.98 (m, 4H), 0.92 ppm (t, $J = 7.4$ Hz, 12H); ^{13}C NMR (75 MHz, $CDCl_3$) δ 132.63, 132.16, 131.46, 129.15, 124.55, 121.52, 55.99, 32.18, 31.72, 29.14, 26.93, 22.57, 14.06 ppm; MALDI-TOF *m/z*. $[M]^-$ calc. for $C_{34}H_{26}Br_4N_2O_4$ 841.8626, found 841.8628; UV vis (CH_2Cl_2), λ max/nm (log ε): 394 (3.98), 413 (3.8), 443 (4.07), 473 (4.45), 507 (4.6); FT-IR (KBr pellet): υ max 2961, 2874, 1707, 1672, 1590, 1567, 1538, 1334, 1223, 808 cm^{-1}

Synthesis of N,N′-di(ethylpropyl)-2,5,8,11-tetrachloroperylene-3,4:9,10-bis(dicarboximide) (**PBI 9**).

A mixture of dioxane (15 mL), methanol (6 mL) and water (3 mL) was added, under inert conditions, to *N,N′*-di(ethylpropyl)-2,5,8,11-tetra(4′,4′,5′,5′-tetramethyl-1′,3′,2′-dioxaborolan-2′-yl)perylene-3,4:9,10-bis(dicarboximide) (250 mg, 0.28 mmol), and $CuCl_2$ (380 g, 2.3 mol). The reaction was refluxed 16 h at 120 °C, and after cooling, it was extracted with toluene. The organic layer was dried over anhydrous sodium sulfate, filtered and evaporated. Purification was carried out by silica gel column chromatography using dichloromethane as eluent.

Yield: 16% (30 mg); orange solid; ^{1}H NMR (300 MHz, $CDCl_3$) δ 8.55 (s, 4H), 5.06 (m, 2H), 2.21 (m, 4H), 1.98 (m, 4H), 0.94 ppm (t, $J = 7.5$ Hz, 12H); ^{13}C NMR (75 MHz, $CDCl_3$) δ; 141.14, 132.44, 128.09, 123.70, 119.97, 58.63, 29.69, 24.93, 11.41 ppm; MALDI-TOF *m/z*. $[M]^-$ calc. for $C_{34}H_{26}N_2O_4Cl_4$ 666.0641, found 666.0087; UV vis (CH_2Cl_2), λ max/nm (log ε): 391 (3.9), 415 (3.8), 443 (4.1), 472 (4.5), 502 (4.7); FT-IR (KBr pellet): υ max 2967, 2934, 2924, 1704, 1664, 1595, 1574, 1330, 1261, 1099, 1022, 816, 802 cm^{-1}

Synthesis of N,N′-di(ethylpropyl)-2,5,8,11-tetra(pyrrolidin-1′-yl) perylene-3,4:9,10-bis(dicarboximide) (**PBI 11**).

Pyrrolidine (85 mg, 1.2 mmol), CsF (182 mg, 1.2 mmol) and 18-crown-6 (720 mg, 4.8 mmol) were added to a solution of N,N′-di(ethylpropyl)-2,5,8,11-tetrabromoperylene-3,4:9,10-tetracarboxydiimide (100 mg, 0.12 mmol) in dry THF (2 mL) in a cone-shaped flask. The reaction was refluxed 24 h under argon atmosphere, and after cooling, it was extracted with dichloromethane. The organic layer was dried over anhydrous sodium sulfate, filtered and evaporated. Purification was carried out by silica gel column chromatography using dichloromethane as eluent.

Yield: 76% (73 mg); red solid; ^{1}H NMR (300 MHz, $CDCl_3$) δ 7.69 (s, 4H), 5.02 (m, 2H), 3.56 (br, 16H), 2.34 (m, 4H), 2.05 (br, 16H), 1.85 (m, 4H), 0.92 ppm (t, $J = 7.4$ Hz, 12H); ^{13}C NMR (75 MHz, $CDCl_3$) δ 167.74, 150.79, 133.89, 133.86, 133.82, 132.45, 130.87, 128.79, 113.05, 107.78, 68.15, 57.66, 52.04, 38.73, 31.95, 30.35, 28.91, 26.00, 25.87, 23.74, 22.97, 22.68, 14.03, 11.66, 10.95 ppm; MALDI-TOF *m/z*. $[M]^-$ calc. for $C_{50}H_{58}N_6O_4$ 806,4520, found 806.4640; UV vis (CH_2Cl_2), λ max/nm (log ε): 336 (4.4), 363 (4.3), 392 (4.1), 507 (4.8); FT-IR (KBr pellet): υ max 2961, 2926, 2868, 1660, 1573, 1631, 1526, 1421, 1299, 1194, 1118, 1088, 948, 826 cm^{-1}

Synthesis of N,N′-di(ethylpropyl)-2,5,8,11-tetrakis(2′,6′-diphenylphenoxy) perylene-3,4:9,10-bis(dicarboximide) (**PBI 12**).

2,6-diphenylphenol (420 mg, 1.68 mmol), CsF (182 mg, 1.2 mmol) and 18-crown-6 (720 mg, 4.8 mmol) were added to a solution of *N,N′*-di(ethylpropyl)-2,5,8,11-tetrabromoperylene-3,4:9,10-tetracarboxydiimide (100 mg, 0.12 mmol) in dry THF (2 mL) in a cone-shaped flask. The reaction was refluxed 24 h under argon atmosphere, and after cooling, it was extracted with dichloromethane. The organic layer was dried over anhydrous sodium sulfate, filtered and evaporated. Purification was carried out by silica gel column chromatography using dichloromethane as eluent.

Yield: 60% (110 mg); orange solid; ^{1}H NMR (300 MHz, $CDCl_3$) δ 7.66 (m, 4H), 7.55 (m, 8H), 7.43 (m, 16H), 7.08 (m, 24H), 6.52 (s, 4H), 5.08 (m, 2H), 2.30 (m, 4H), 1.93 (m, 4H), 0.92 ppm (t, $J = 7.4$ Hz, 12H); ^{13}C NMR (75 MHz, $CDCl_3$) δ 159.45, 146.71, 136.84, 136.83, 135.56, 133.31, 132.75, 130.86, 129.00, 128.08, 127.55, 127.00, 116.21, 109.29, 107.71, 56.40, 24.92, 11.33 ppm; MALDI-TOF *m/z*. $[M]^-$ calc. for $C_{106}H_{78}N_2O_8$ 1506.576366, found 1506.5783; UV vis (CH_2Cl_2), λ max/nm (log ε): 421 (4.4), 459 (4.3), 492 (4.6), 531 (4.8); FT-IR (KBr pellet): υ max 3061, 3031, 2961, 2961, 2921, 2851, 1689, 1654, 1567, 1462, 1415, 1380, 1345, 1316, 1229, 1194, 1065, 908, 762, 698 cm^{-1}

Synthesis of N,N′-di(hexylheptyl)-2,5,8,11-tetra(p-tolylethynyl)perylene-3,4:9,10-bis(dicarboximide) (**PBI 16**).

A solution of *N,N′-di(hexylheptyl)*-2,5,8,11-tetrabromoperylene-3,4:9,10-tetracarboxydiimide (20 mg, 0.019 mmol) and dry triethylamine (10 mL) in dry THF (10 mL) was added under argon to a mixture of $Pd(PPh_3)_4$ (4 mg, 0.0035 mmol) and CuI (0.5 mg, 0.0026 mmol), followed by the addition of *p*-tolylacetylene (24 mL, 17.4 mg, 0.15 mmol). The mixture was refluxed overnight. After cooling to room temperature, the mixture was diluted with methylene chloride and treated with conc. HCl (14 mL) and water (7 mL). The organic layer was dried over anhydrous magnesium sulfate, filtered and evaporated. Purification was carried out by silica gel column chromatography using toluene as eluent.

Yield: 91% (21 mg); red solid; ^{1}H NMR (300 MHz, $CDCl_3$) δ 8.71 (s, 4H), 7.74 (d, $J = 8.0$ Hz, 8H), 7.31 (d, $J = 8.0$ Hz, 8H), 5.25 (m, 2H), 2.48 (s, 12H), 2.34 (m, 4H), 2.01 (m, 4H), 1.41–1.31 (m 12H), 0.89 ppm (m 12H); ^{13}C NMR (75 MHz, CD_2Cl_4, 70 °C) δ 161.95, 139.75, 132.28, 131.89, 130.68, 129.19, 128.74, 128.35, 127.74, 124.41, 123.38, 119.92, 100.55, 90.04, 54.74, 32.35, 31.62, 29.13, 26.94, 22.47, 21.54, 13.90 ppm; MALDI-TOF *m/z*. $[M]^-$ calc. for $C_{86}H_{86}N_2O_4$: 1210.659; found 1210.650; UV vis (CH_2Cl_2), λ max/nm (log ε): 332 (4.78), 493 (4.63), 532 (4.64).; FT-IR (KBr pellet): υ max 3448, 2924, 2854, 2133, 1900, 1691, 1645, 1601, 1503, 1642, 1377, 1270, 1174, 1115, 1037, 964, 809, 522 y 408 cm^{-1}

Synthesis of N,N′-di(hexylheptyl)-2,5,8,11-tetra(pyrrolidin-1′-yl) perylene-3,4:9,10-bis(dicarboximide) (**PBI 18**).

Pyrrolidine (85 mg, 1.2 mmol), CsF (182 mg, 1.2 mmol) and 18-crown-6 (720 mg, 4.8 mmol) were added to a solution of *N,N′-di(hexylheptyl)*-2,5,8,11-tetrabromoperylene-3,4:9,10-tetracarboxydiimide

(130 mg, 0.12 mmol) in dry THF (2 mL) in a cone-shaped flask. The reaction was refluxed 24 h under argon atmosphere, and after cooling, it was extracted with dichloromethane. The organic layer was dried over anhydrous sodium sulfate, filtered and evaporated. Purification was carried out by silica gel column chromatography using dichloromethane as eluent.

Yield: 81% (100 mg); red solid; ^{1}H NMR (300 MHz, $CDCl_3$) δ 7.69 (s, 4H),5.17 (m, 2H), 3.56 (br, 16H), 2.41 (m, 4H), 2.06 (br, 16H), 1.75 (m, 4H), 1.21 (br, 32H), 0.8 ppm (t, $J = 7.3$ Hz, 12H); ^{13}C NMR (75 MHz, $CDCl_3$) δ 164.36, 163.48, 150.96, 150.63, 133.79, 113.04, 107.74, 104.74, 54.55, 52.11, 33.32, 31.90, 29.37, 27.16, 25.93, 22.60, 14.07 ppm; MALDI-TOF *m/z*. $[M]^-$ calc. For $C_{66}H_{90}N_6O_4$ 1030.7029, found 1030.7024; UV vis (CH_2Cl_2), λ max/nm (log ε): 337 (4.4), 363 (4.3), 393 (4.1), 507 (4.8); FT-IR (KBr pellet): υ max 2950, 2921, 2845, 1666, 1614, 1567, 1526, 1439, 1415, 1310, 1199, 1112, 943, 826 cm^{-1}.

Synthesis of N,N′-bis(3′-trimethylammoniumprop-1′-yl)perylene-3,4:9,10-bis(dicarboximide) tetrabromide (**PBI 21**).

Hydrobromic acid (15 mL) was added over *N,N′*-bis(3′-trimethylammoniumprop-1′-yl)perylene-3,4:9,10-bis(dicarboximide) di-*p*-toluenesulfonate [54] (2g, 0.002 mol) and heated at 80 °C during 45 min. After cooling, the product was precipitated with acetone and then filtered and dried. The limited solubility of the compound precluded the obtaining of a useful ^{13}C NMR spectrum.

Yield: 81% (1.3g); red solid; ^{1}H NMR (300 MHz, DMSO-d_6) δ 8.85 (d, $J = 8.2$ Hz, 4H), 8.51 (d, $J = 7.9$ Hz, 4H), 4.09 (m, 4H), 2.96 (s, 18H), 2.09 ppm (m, 8H); ESI HRMS *m/z*. $[M]^{+2}$ calc. for $C_{36}H_{38}N_4O_4^{2+}$ 295.1441, found 295.1433; UV vis (CH_2Cl_2), λ max/nm (log ε): 464 (4.1), 493 (4.6), 526 (4.8); FT-IR (KBr pellet): υ max 3020, 2956, 2337, 1689, 1643, 1584, 1468, 1444, 1339, 1240, 814, 744 cm^{-1}

3.1. Contact angle measurements

PBI solutions were prepared at a concentration of 2 mg/mL in DCM. For PBI **5,** additionally 3 drops of TFA were added. Series 3 were prepared from methanol instead. The glass substrates (Ted Pella round glass coverslips) were previously cleaned with acetone. Drop casting was performed with a 50 μL Eppendorf pippete. Spin coating samples were prepared with different velocities and finally optimized to 25 rps. The concentration of the solutions for spin coating was raised to 4 mg/mL to increase the thickness of the films.

The contact angles were measured with Dataphysics OCA 25 contact angle measurement device. The dosing volume and dosing speed for each solvent is specified in the supporting information (Table S1). The solvent properties used for the energies calculations are also described in the SI (Table S2).

4. Conclusions

These results present systematically and consistently data about the wetting-structure relationship of the selected PBI coatings, furthermore numerous correlations between the structural substituents descriptors and the wettability and surface energy have been established. The QSPR analysis on the surface wettability and surface energy will lay the groundwork for guiding the molecular design of PBIs in order to tune the interfacial interaction as demanded by the specific applications. We believe that the use of different models helps in understanding the different contributions. Finally, the most striking result suggests that contrary to colorimetric/spectroscopic properties, the imide position plays a decisive role in surface wettability.

CRediT authorship contribution statement

M. Eugenia Pérez-Ojeda: Investigation, Writing – original draft, Conceptualization, Supervision, Writing – review & editing, Funding acquisition. **Nathalie Zink-Lorre:** Investigation, organic synthesis, characterization, Writing – original draft. **Sara Pla:** Investigation. **Andreas Zink:** Investigation, wettability characterization. **Ángela Sastre-Santos:** Supervision, Writing – review & editing, Funding acquisition. **Fernando Fernández-Lázaro:** Conceptualization, Supervision, Writing – review & editing, Funding acquisition. **Andreas Hirsch:** Supervision, Writing – review & editing, Funding acquisition.

Declaration of competing interest

The authors declare that they have no known competing financial interests or personal relationships that could have appeared to influence the work reported in this paper.

Acknowledgements

This work was supported by the Deutsche Forschungsgemeinschaft (DFG; DFG—SFB 953 "Synthetic Carbon Allotropes" projects A1 and A9) and by the European Regional Development Fund "A way to make Europe" and the Spanish Ministerio de Ciencia e Innovación/Agencia Estatal de Investigación (PID2019-109200 GB-I00). M.E.P–O. acknowledges support by " Emerging Talents Initiative (ETI) of FAU Friedrich Alexander Universität Erlangen-Nürnberg. The authors are grateful to Dr. P. Ertl for his advice regarding substituents descriptors calculation and to Prof. Dr. M. Halik for the use of the optical contact angle device at the Interdisciplinary Center for Nanostructured Films (IZNF).

Appendix A. Supplementary data

Supplementary data to this article can be found online at https://doi.org/10.1016/j.dyepig.2021.110044.

References

[1] Nowak-Król A, Würthner F. Progress in the synthesis of perylene bisimide dyes. Organic Chem Front 2019;6(8):1272–318. https://doi.org/10.1039/C8QO01368C.
[2] Würthner F, Saha-Möller CR, Fimmel B, Ogi S, Leowanawat P, Schmidt D. Perylene bisimide dye assemblies as archetype functional supramolecular materials. Chem Rev 2016;116(3):962–1052. https://doi.org/10.1021/acs.chemrev.5b00188.
[3] Shi Q, Wu J, Wu X, Peng A, Huang H. Perylene diimide-based conjugated polymers for all-polymer solar cells. Chem Eur J 2020;26(55):12510–22. https://doi.org/10.1002/chem.202001011.
[4] Zink-Lorre N, Font-Sanchis E, Sastre-Santos Á, Fernández-Lázaro F. Perylenediimides as more than just non-fullerene acceptors: versatile components in organic, hybrid and perovskite solar cells. Chem Commun 2020;56(27):3824–38. https://doi.org/10.1039/D0CC00337A.
[5] Matussek M, Filapek M, Gancarz P, Krompiec S, Grzegorz Małecki J, Kotowicz S, et al. Synthesis and photophysical properties of new perylene bisimide derivatives for application as emitting materials in OLEDs. Dyes Pigments 2018;159:590–9. https://doi.org/10.1016/j.dyepig.2018.07.006.
[6] Golshan M, Rostami-Tapeh-Esmail E, Salami-Kalajahi M, Roghani-Mamaqani H. A review on synthesis, photophysical properties, and applications of dendrimers with perylene core. Eur Polym J 2020;137:109933. https://doi.org/10.1016/j.eurpolymj.2020.109933.
[7] Muñoz-Mármol R, Boj PG, Villalvilla JM, Quintana JA, Zink-Lorre N, Sastre-Santos Á, et al. Effect of substituents at imide positions on the laser performance of 1,7-bay-substituted perylenediimide dyes. J Phys Chem C 2021;125(22):12277–88. https://doi.org/10.1021/acs.jpcc.1c00833.
[8] Casillas R, Papadopoulos I, Ullrich T, Thiel D, Kunzmann A, Guldi DM. Molecular insights and concepts to engineer singlet fission energy conversion devices. Energy Environ Sci 2020;13(9):2741–804. https://doi.org/10.1039/D0EE00495B.
[9] Papadopoulos I, Gutiérrez-Moreno D, McCosker PM, Casillas R, Keller PA, Sastre-Santos A, et al. Perylene-Monoimides: singlet fission down-conversion competes with up-conversion by geminate triplet–triplet recombination. J The Journal of Physical Chemistry A 2020;124(28):5727–36.
[10] Zhang F, Li W, Jiang T, Li X, Shao Y, Ma Y, et al. Real roles of perylene diimides for improving photocatalytic activity. RSC Adv 2020;10(39):23024–37. https://doi.org/10.1039/D0RA03421E.
[11] Chand S, Pandey AK, Singh R, Singh KN. Visible-light-induced photocatalytic oxidative decarboxylation of cinnamic acids to 1,2-diketones. J Org Chem 2021;86(9):6486–93. https://doi.org/10.1021/acs.joc.1c00322.
[12] Ghosh I, Ghosh T, Bardagi JI, König B. Reduction of aryl halides by consecutive visible light-induced electron transfer processes. Science 2014;346(6210):725. https://doi.org/10.1126/science.1258232.
[13] McDowall D, Greeves BJ, Clowes R, McAulay K, Fuentes-Caparrós AM, Thomson L, et al. Controlling photocatalytic activity by self-assembly – tuning perylene bisimide photocatalysts for the hydrogen evolution reaction. Adv Energy Mater 2020;10(46):2002469. https://doi.org/10.1002/aenm.202002469.

[14] Backes C, Hauke F, Hirsch A. The potential of perylene bisimide derivatives for the solubilization of Carbon nanotubes and graphene. Adv Mater 2011;23(22–23): 2588–601. https://doi.org/10.1002/adma.201100300.
[15] Wild S, Lloret V, Vega-Mayoral V, Vella D, Nuin E, Siebert M, et al. Monolayer black phosphorus by sequential wet-chemical surface oxidation. RSC Adv 2019;9 (7):3570–6. https://doi.org/10.1039/C8RA09069F.
[16] Abellán G, Lloret V, Mundloch U, Marcia M, Neiss C, Görling A, et al. Noncovalent functionalization of black phosphorus. Angew Chem Int Ed 2016;55(47): 14557–62. https://doi.org/10.1002/anie.201604784.
[17] Micheli E, D'Ambrosio D, Franceschin M, Savino M. Water soluble cationic perylene derivatives as possible telomerase inhibitors: the search for selective G-quadruplex targeting. Mini Rev Med Chem 2009;9(14):1622–32.
[18] You S, Cai Q, Zheng Y, He B, Shen J, Yang W, et al. Perylene-cored star-shaped polycations for fluorescent gene vectors and bioimaging. ACS Appl Mater Interfaces 2014;6(18):16327–34. https://doi.org/10.1021/am5045967.
[19] Zhou W, Liu G, Yang B, Ji Q, Xiang W, He H, et al. Review on application of perylene diimide (PDI)-based materials in environment: pollutant detection and degradation. Sci Total Environ 2021;780:146483. https://doi.org/10.1016/j.scitotenv.2021.146483.
[20] Calvo-Gredilla P, García-Calvo J, Cuevas JV, Torroba T, Pablos J-L, García FC, et al. Solvent-Free off-on detection of the improvised explosive triacetone triperoxide (TATP) with fluorogenic materials. Chem Eur J 2017;23(56):13973–9. https://doi.org/10.1002/chem.201702412.
[21] Song K, Lee J, Choi S-O, Kim J. Interaction of surface energy components between solid and liquid on wettability, and its application to textile anti-wetting finish. Polymers 2019;11(3):498.
[22] Liang Y, Wang H, Wang D, Liu H, Feng S. The synthesis, morphology and liquid-crystalline property of polysiloxane-modified perylene derivative. Dyes Pigments 2012;95(2):260–7. https://doi.org/10.1016/j.dyepig.2012.04.015.
[23] Luo Z, Wu F, Zhang T, Zeng X, Xiao Y, Liu T, et al. Designing a perylene diimide/fullerene hybrid as effective electron transporting material in inverted perovskite solar cells with enhanced efficiency and stability. Angew Chem Int Ed 2019;58(25): 8520–5. https://doi.org/10.1002/anie.201904195.
[24] Ye Y, Lü B, Cheng W, Wu Z, Wei J, Yin M. Controllable self-assembly of amphiphilic zwitterionic PBI towards tunable surface wettability of the nanostructures. Chem Asian J 2017;12(9):1020–4. https://doi.org/10.1002/asia.201700246.
[25] Berner NC, Winters S, Backes C, Yim C, Dümbgen KC, Kaminska I, et al. Understanding and optimising the packing density of perylene bisimide layers on CVD-grown graphene. Nanoscale 2015;7(39):16337–42. https://doi.org/10.1039/C5NR04772B.
[26] Li M, Lv J, Wang L, Liu J, Yu X, Xing R, et al. An alcohol-soluble perylene diimide derivative as cathode interfacial layer for PDI-based nonfullerene organic solar cells. Colloids Surf A Physicochem Eng Asp 2015;469:326–32. https://doi.org/10.1016/j.colsurfa.2015.01.017.
[27] Jiang K, Wu F, Yu H, Yao Y, Zhang G, Zhu L, et al. A perylene diimide-based electron transport layer enabling efficient inverted perovskite solar cells. J Mater Chem 2018;6(35):16868–73. https://doi.org/10.1039/C8TA06081A.
[28] Sriramulu D, Turaga SP, Bettiol AA, Valiyaveettil S. Oriented perylene incorporated optically anisotropic 2D silica films. RSC Adv 2017;7(52):32692–702. https://doi.org/10.1039/C7RA05036D.
[29] Madhurima V, Priyanka KG, Pavan KSND, Nagarajan S. Analysis of wetting of perylene diimide thin films-on-glass by water. 594-595 Key Eng Mater 2014: 1074–7. https://doi.org/10.4028/www.scientific.net/KEM.594-595.1074.
[30] Chen Z, Debije MG, Debaerdemaeker T, Osswald P, Würthner F. Tetrachloro-substituted perylene bisimide dyes as promising n-type organic semiconductors: studies on structural, electrochemical and charge transport properties. ChemPhysChem 2004;5(1):137–40. https://doi.org/10.1002/cphc.200300882.
[31] Li X-M, Reinhoudt D, Crego-Calama M. What do we need for a superhydrophobic surface? A review on the recent progress in the preparation of superhydrophobic surfaces. J Chem Soc Rev 2007;36(8):1350–68.
[32] Owens DK, Wendt RC. Estimation of the surface free energy of polymers. J Appl Polym Sci 1969;13(8):1741–7. https://doi.org/10.1002/app.1969.070130815.
[33] Ertl P. A web tool for calculating substituent descriptors compatible with Hammett sigma constants.
[34] White DP, Anthony JC, Oyefeso AO. Computational measurement of steric effects: the size of organic substituents computed by ligand repulsive energies. J Org Chem 1999;64(21):7707–16. https://doi.org/10.1021/jo982405w.
[35] Charton M. Steric effects. I. Esterification and acid-catalyzed hydrolysis of esters. J Am Chem Soc 1975;97(6):1552–6.
[36] Charton M. Steric effects. 7. Additional V constants. J Org Chem 1976;41(12): 2217–20.
[37] Harper KC, Bess EN, Sigman MS. Multidimensional steric parameters in the analysis of asymmetric catalytic reactions. J Nature chem 2012;4(5):366–74.
[38] Wei W, Ouyang S, Zhang T. Perylene diimide self-assembly: from electronic structural modulation to photocatalytic applications. J Semiconduct 2020;41(9): 091708. https://doi.org/10.1088/1674-4926/41/9/091708.
[39] Marcia M, Hirsch A, Hauke F. Perylene-based non-covalent functionalization of 2D materials. FlatChem 2017;1:89–103. https://doi.org/10.1016/j.flatc.2017.01.001.
[40] Nakamura T, Shioya N, Shimoaka T, Nishikubo R, Hasegawa T, Saeki A, et al. Molecular orientation change in naphthalene diimide thin films induced by removal of thermally cleavable substituents. Chem Mater 2019;31(5):1729–37. https://doi.org/10.1021/acs.chemmater.8b05237.
[41] Kalin M, Polajnar M. The wetting of steel, DLC coatings, ceramics and polymers with oils and water: the importance and correlations of surface energy, surface tension, contact angle and spreading. Appl Surf Sci 2014;293:97–108. https://doi.org/10.1016/j.apsusc.2013.12.109.
[42] Stiegler LMS, Luchs T, Hirsch A. Shell-by-Shell functionalization of inorganic nanoparticles. Chem Eur J 2020;26(39):8483–98. https://doi.org/10.1002/chem.202000195.
[43] https://www.tstar.com/blog/bid/33845/surface-energy-of-plastics.
[44] Demmig S, Langhals H. Leichtlösliche, lichtechte perylen-fluoreszenzfarbstoffe. Chem Ber 1988;121(2):225–30. https://doi.org/10.1002/cber.19881210205.
[45] Deligeorgiev T, Zaneva D, Petkov I, Timcheva I, Sabnis R. Synthesis and properties of fluorescent bis-quaternized perylene dyes. Dyes Pigments 1994;24(1):75–81. https://doi.org/10.1016/0143-7208(94)87012-8.
[46] Deyama K, Tomoda H, Muramatsu H, Matsui M. 3, 4, 9, 10-Perylenetetracarboxdiimides containing perfluoroalkyl substituents. Dyes Pigments 1996;30(1):73–8.
[47] Nagao Y, Naito T, Abe Y, Misono T. Synthesis and properties of long and branched alkyl chain substituted perylenetetracarboxylic monoanhydride monoimides. Dyes Pigments 1996;32(2):71–83. https://doi.org/10.1016/0143-7208(96)00017-4.
[48] Maiti DK, Roy S, Datta A, Banerjee A. Aqueous fluoride ion sensing by a new perylenediimide derivative: interaction between the hydrated fluoride and the aromatic molecule. Chem Phys Lett 2013;588:76–81. https://doi.org/10.1016/j.cplett.2013.09.056.
[49] Mahata K, Frischmann PD, Würthner F. Giant electroactive M4L6 tetrahedral host self-assembled with Fe(II) vertices and perylene bisimide dye edges. J Am Chem Soc 2013;135(41):15656–61. https://doi.org/10.1021/ja4083039.
[50] Battagliarin G, Zhao Y, Li C, Müllen K. Efficient tuning of LUMO levels of 2,5,8,11-substituted perylenediimides via copper catalyzed reactions. Org Lett 2011;13(13): 3399–401. https://doi.org/10.1021/ol201144w.
[51] Teraoka T, Hiroto S, Shinokubo H. Iridium-Catalyzed direct tetraborylation of perylene bisimides. Org Lett 2011;13(10):2532–5. https://doi.org/10.1021/ol2004534.
[52] Zink-Lorre N, Font-Sanchis E, Sastre-Santos Á, Fernández-Lázaro F. Fluoride-mediated alkoxylation and alkylthio-functionalization of halogenated perylenediimides. Organic Chem Front 2017;4(10):2016–21. https://doi.org/10.1039/C7QO00337D.
[53] Zhang Z-G, Qi B, Jin Z, Chi D, Qi Z, Li Y, et al. Perylene diimides: a thickness-insensitive cathode interlayer for high performance polymer solar cells. Energy Environ Sci 2014;7(6):1966–73. https://doi.org/10.1039/C4EE00022F.
[54] Soroka PV, Vakhnin AY, Skryshevskiy YA, Boiko OP, Anisimov MI, Slominskiy YL, et al. Charge carrier trapping in highly-ordered lyotropic chromonic liquid crystal films based on ionic perylene diimide derivatives. Eur Phys J Appl Phys 2014;68 (3):30201. https://doi.org/10.1051/epjap/2014140272.